Proceedings of the International Symposium on Engineering Lessons Learned from
the 2011 Great East Japan Earthquake, March 1-4, 2012, Tokyo, Japan

TOHOKU TSUNAMI SURVEY, MODELING AND PROBABILISTIC LOAD ESTIMATION APPLICATIONS

Solomon C. YIM[1], Kwok Fai CHEUNG[2,] Michael J. OLSEN[3], and Yoshiki YAMAZAKI[4]

[1] Professor, School of Civil and Construction Engineering, Oregon State University, Corvallis, OR, USA, solomon.yim@oregonstate.edu
[2] Professor, Ocean and Resources Engineering, University of Hawaii at Manoa, Honolulu, HI, USA, cheung@hawaii.edu
[3] Assistant Professor, School of Civil and Construction Engineering, Oregon State University, Corvallis, OR, USA, michael.olsen@oregonstate.edu
[4] Post-doctoral Research Fellow, Ocean and Resources Engineering, University of Hawaii at Manoa, Honolulu, HI, USA, yoshikiy@hawaii.edu

ABSTRACT: The Tohoku earthquake (Mw = 9.0) and tsunami inflicted substantial damage to coastal infrastructure throughout Japan. Extensive seismic networks, geodetic instruments, and water-level stations provided unprecedented, detailed datasets to record the event for scientific research. The data allows accurate modeling of the near-field tsunami using the non-hydrostatic model NEOWAVE to understand the impact along the Tohoku coast. A ground-based LIDAR survey captured damage to structures and the overall topography at several sites for inundation modeling. The high-resolution LIDAR data provides critical geospatial information to link field observations, topographic mapping, and structural damage to feed and validate tsunami and structural load models. The dense quantity of measurements enables one not only to virtually explore the site, but also improves quantification of damage. An analysis plan to develop a better understanding of tsunami loads on structures using the model data and observations is described. This plan includes immediate, specific deterministic analysis and experiments needed to calibrate tsunami inundation models for built environment as well as a comprehensive probability-based tsunami load-estimation procedure.

Key Words: Tohoku earthquake, tsunami modeling, LIDAR survey, analysis plan, and probability-based load estimate

INTRODUCTION

The Tohoku earthquake (Mw = 9.0) and tsunami inflicted substantial damage to coastal infrastructure throughout Japan. Extensive seismic networks, geodetic instruments, and water-level stations provided unprecedented datasets of the event for scientific research. Figure 1 shows the location of the epicenter and the buoys, which recorded clear signals of the tsunami along the Tohoku and Hokkaido coasts. These datasets enable modeling of the near-field tsunami directly from the earthquake rupture and

validation of the results with water-level and geodetic measurements (Yamazaki *et al*., 2011). The validated model of the tsunami provides important flow data to interpret damage and destruction along the Tohoku coast.

The damage and destruction were widespread throughout many of the areas inundated by the devastating tsunami. A team of Japanese scientists surveyed the tsunami flow depth and runup immediately after the event (Mori *et al.*, 2011). Several coordinated surveys were conducted by international teams to collect valuable time-sensitive quantitative information to improve understanding of structural response to tsunami loading. One survey included high-resolution, ground-based Light Detection and Ranging (LIDAR) to collect dense topographic and structural data, which includes deformations of partial concrete wall blow-outs, scour depths and volumes, and lateral and longitudinal displacement in damaged steel frame structures at a wastewater treatment facility. Additional sites highlight other structural failures such as collapses of bridges, and overturning of retaining walls. The dense quantity of measurements enables one not only to virtually explore the site, but also improves quantification of damage.

The 2011 Tohoku event has demonstrated the destructive power of tsunamis and the need to develop a systematic procedure for definition of load conditions and design of coastal infrastructure. The accurate reproduction of the near-field tsunami by Yamazaki et al. (2011) and the high-resolution LIDAR data enable a post-event assessment to quantify and understand tsunami loading, structural response, and failure mode for development of a rigorous design methodology. In this paper, we describe modeling of the near-field tsunami from seismic data, provide a brief description of the LIDAR survey of topography and structural damage along the Tohoku coast, and a framework to utilize the modeled and measured data for calibration of deterministic and probabilistic models for tsunami hazard analysis.

POST-EVENT ASSESSMENT OF TSUNAMI IMPACT

The 2011 Tohoku tsunami was generated by a powerful Mw 9.0 earthquake near the Japan Trench. We utilized NEOWAVE (Non-hydrostatic Evolution of Ocean Wave) to model the near-field tsunami from its generation with the earthquake rupture to the impact of the resulting waves along the Japanese coast. The staggered, finite-difference model builds on the nonlinear shallow-water equations with a vertical velocity term to account for weakly-dispersive waves and a momentum conservation scheme to describe bores or hydraulic jumps (Yamazaki *et al.*, 2009, 2011a).

The computation utilized two levels of two-way nested grids. The level-1 grid extends from the Kamchatka Peninsula to Okinawa at 2 arc-min (~3,000 m) resolution to describe tsunami propagation along the continental margin and to provide an open boundary for the waves leaving the computational domain. The level-2 grid, which covers the region depicted in Figure 1, resolves the rupture models, large-scale coastal features, and near-field tsunami waves at 24 arc-sec (~600 m). Inundation is not considered at this resolution and a vertical wall condition is imposed at the coastline. The bathymetry is derived from the 1 arc min (~1,500 m) ETOPO1 data and the 20 arc sec (~475 m) data from the Japan Meteorological Agency (JMA). The digital elevation model is in geodetic coordinates using the WGS84 datum and elevation is referenced to a geoid model of mean sea level.

The ground shaking from the earthquake lasted 140 seconds (2 min 20 sec). Figure 2 shows the slip distribution, seafloor deformation, and tsunami waves at the end of the rupture. Yamazaki *et al.* (2011b) inferred the slip time history from finite-fault inversion of the seismic P waves and forward modeling of the near-field tsunami records. The model comprises 20 × 20 km^2 subfaults with strike and dip angles of 192° and 12° and utilizes the epicenter (38.107°N, 142.916°E) and origin time 14:46:18.14 UTC from Zhao *et al.* (2011). The 70-m slip near the trench corroborates findings from GPS data (*e.g.*, Ito *et al.*, 2011; and Simons *et al.*, 2011). Implementation of the finite-fault solution in the planar fault model of Okada (1985) provides the time history of seafloor deformation. The vertical seafloor displacement shows a distinct pattern of uplift on the continental margin and subsidence on the shelf. The vertical velocity term in NEOWAVE facilitates modeling of tsunami generation and

transfer of kinetic energy from the seafloor deformation and thus provides a more realistic description of the near-field tsunami.

The computation covers 6 hours of elapsed time with 1 and 0.5-s time steps in the level-1 and 2 grid and output intervals of 1 min. Figure 3 shows good agreement of the computed and recorded water elevations at the nearshore buoys. The signals at the Kushiro, Tomakomai, and Mutsu Ogawara wave buoys, which are located in shallow water of 20 to 50 m, are strongly influenced by local features. The GPS buoys at 100 to 300 m water depth recorded the clear signals of the tsunami. The initial wave has the largest impact to the Tohoku coast adjacent to the rupture zone. The sensitivity analysis of Yamazaki *et al.* (2011b) indicates that the large seafloor displacement along the trench is responsible for the 6 m wave amplitude recorded at the central and south Iwate GPS buoys. All buoys show persistent oscillations of the water levels. Both the time series and spectra vary significantly along the coasts indicating local amplification of frequency components over the continental margin and embayments. The signals between 100 to 200 min are due to large-scale standing edge waves along the Pacific margin coasts, as observed during the 2010 Chile tsunami (Yamazaki and Cheung, 2011).

The modeled event is compatible with seismic data from around the world as well as recorded geodetic and tsunami data along the Japan coasts. Figure 4 shows the computed maximum surface elevation using the level-2 grid and the recorded runup from Mori *et al.* (2011). The model shows focusing of energy at Fukushima and Iwate with typical wave amplitude of 10 to 15 m along the coasts corroborating the recorded surface elevation on land. The impact was exacerbated by 1 to 2 m subsidence of the coastlines at the hardest hit areas. The Iwate coastline consists of coves and narrow embayments with steep cliffs that resulted in channeling of wave energy and large runup heights of close to 40 m at a number of locations. High-resolution topography, bathymetry, and an additional level of nested grids along the coastline are necessary for NEOWAVE to reproduce the recorded runup data.

LIDAR SURVEY OF TSUNAMI-INDUCED STRUCTURAL DAMAGE

LIDAR Topographic Mapping

LIDAR is a line-of-sight technology that emits laser pulses at defined, horizontal and vertical angular increments to produce a point cloud, containing XYZ coordinates for objects that return a portion of the light pulse. Details of typical ground-based LIDAR (also called 3D laser scanning) acquisition, processing, and post-earthquake applications can be found in Kayen *et al.* (2010), Olsen *et al.* (2010, 2011, 2012a&b) and Olsen and Donahue (2011). Additional LIDAR work completed in Japan following the earthquake and tsunami was performed by Kayen *et al.* (2011). Messinger *et al.* (2010) discussed the importance of LIDAR data in relief efforts and identifying damage.

Survey overview

The 3D laser scan survey following the Tohoku earthquake and tsunami was performed in June and July 2011 consisting of a team of U.S.-based and Japanese researchers. Table 1 lists the key sites surveyed, which were selected based on observations made during previous surveys. Sites were selected for topographic mapping in valleys such as Onagawa. Additional scans were completed to document structural damage and deformations at several buildings impacted by the tsunami. A typical setup consists of the 3D laser scanner with a camera and GNSS receiver mounted above the scanner. The Riegl VZ-400 laser scanner can acquire data up to a range of 300-500 m, depending on object reflectivity and scan mode. GPS coordinates were obtained for many scans; however, the team did not have access to GPS correction data for precise positioning. As such, the GPS coordinates were obtained with an estimated, absolute accuracy of approximately 2 m. Fortunately, post-processing through matching features between scans enabled improved relative measurements within the scan data.

Table 1 Locations surveyed with 3D laser scanning

Site	Prefecture	Emphasis	# Scans	Days
Yuriage\Natori	Miyagi	Structural	20	2
Onagawa	Miyagi	Topography	30	3
Gamou (Wastewater Treatment Plant)	Miyagi	Structural	10	1
Minamisanriku	Miyagi	Structural	5	1
Rikuzentakata	Iwate	Structural & Topographic	38	3
Totals			**103**	**10**

Onagawa was selected as an important location for detailed topographic mapping using the ground-based scanner. The city consists of flat terrain (0.2% slope, typical) in narrow valleys surrounded by steep hills. The Onagawa topographic LIDAR data consisted of 22 scans performed at key locations (Figure 5) to obtain coverage throughout each of the narrow valleys that were inundated from the tsunami. In areas where specific structures were of interest for additional modeling, the scans had significant overlap. However, for a few of the scans located at the East sections of the valley or bay, there was minimal overlap between neighboring scans. Hence, there is less ability to validate the geo-referencing quality of those scans.

Prior to the static scan surveys, Asia Air survey Co. performed mobile laser scanning throughout Onagawa, as well as other areas of Japan. The static 3D laser scan data collected through the effort described herein has been combined with their mobile laser scan data to provide more detailed topographic maps. Mobile laser scan data is very dense along the roadways and presents a rapid data acquisition technique to survey damage following an earthquake or tsunami. However, static 3D laser scan data can fill in gaps in locations that are not accessible by vehicle because of more flexibility in selecting an appropriate viewpoint. For example, the research team performed scans at several sites located at high elevations for improved topographic visibility and scanning. This required carrying the equipment up several flights of stairs because of limited access. Unfortunately, the team did not have access to the mobile scan data until after the project, so optimal setup locations to reduce redundancy could not be chosen. Figure 5 also shows the approximate extents of mobile laser scan data coverage.

Because the mobile scan and static scan datasets were collected at different times, the data can also be explored to study recovery efforts. For example, the main highway is 0.5 m higher in elevation in the static scan data, showing a significant reconstruction of the road surface on top of the old road.

In addition to the topographic mapping at Onagawa, several structures were scanned to record deformations from the tsunami impact. Details of the structural analysis performed on similar datasets can be found in Olsen *et al.,* (2012b). Combining LIDAR data with as-built structural drawings enables one to create a numerical model of the structure. Further, one can measure deformation by comparing to estimated initial conditions. The initial condition of most walls can be created by least-squares fitting a plane to points on the undamaged sections of the walls.

LIDAR Processing

This section will discuss the processing of the LIDAR data for use in topographic mapping of Onagawa. Details of processing the data for structural analysis can be found in Olsen *et al.* (2010, 2012). The topographic DEM processing using LIDAR consisted of the following tasks:

a. Pre-processing and filtering to remove noise
b. Scan alignment and geo-referencing
c. Topographic filtering to remove buildings and other structures
d. Coordinate transformation in GIS
e. Creation of a DEM

a. Pre-processing

Because the scan dataset was very large, it was split into 5 sections (north, south, east, west and central) to simplify processing. Prior to alignment and modeling, the point cloud must be processed to remove noise, debris, and sporadic points from the dataset, which would not be consistent between scans. One common problem is that the laser pulses can reflect off of water and wet surfaces, reflect off of another object, and then return to the scanner. Because the scanner only knows the angle at which the pulses were fired, these points become mirrored below the water surface in the dataset. Figure 6(a) shows an example of these spurious points collected in Onagawa. There were many data points resulting from this effect due to the substantial amount of water remaining from the tsunami inundation and recent rain. Moisture in the air and birds also create noise in the dataset. Automatic filters can remove points that do not have a neighboring point within a specified threshold distance. For this dataset, a threshold of 2 m was used.

To help in manual removal of points that cannot be removed by automatic filters, color information from calibrated photographs taken at the same time as the scan is also mapped to the point cloud datasets. To ensure high precision mapping and improvement over the default calibration, fine-tune adjustments can be implemented by selecting common points in the photographs and scans, if desired.

Static scanners operate on fixed angular increments. As such, there are substantially more points close to the scanner origin, which becomes sparser with distance from the scanner. To improve interaction with the dataset and improve pick points used in scan geo-referencing, a minimum separation filter was applied to remove points that were closer than 0.02 m.

b. Scan Alignment and Geo-referencing

Scanners collect each scan in its own reference frame, which only includes objects visible from that position. Each of these scans needs to be converted to a common coordinate system. Olsen (2011) discusses common procedures used to align scans. Typically, target-resection methods are implemented because they generally will provide the highest local accuracy; however, they require additional field time for long-range scanning applications (Williams *et al.* 2012). Given the limited window of time available to collect data and small size of the team, it was not feasible to perform the additional surveying necessary to establish control for the targets. Hence, an alternate approach was implemented.

The mobile laser scan data provided by Asia Air Survey, Co. was geo-referenced using RTK-GPS, producing cm-level accurate data. Hence, their data was used as a reference to geo-reference the static scan data. This data was acquired in a local, Japanese coordinate system, so it was not immediately compatible with the uncorrected GPS positions obtained during the static scans.

Each static scan was first leveled using inclination sensor values obtained during scanning. Then a common feature was identified in the static scan and mobile scan data to translate the static scan into the coordinate system of the mobile scan data. Field note sketches and the relative relationship of the GPS positions were used as a guide. Next, the scans were rotated about the Z-axis to match roughly the mobile scan data. This was completed for all scans overlapping the mobile scan data. For scans that did not overlap the mobile scan data, neighboring static scans were used for reference. Cloud-to-cloud, surface matching (Vosselman and Maas, 2010) techniques were used to align the scans. In areas with substantial overlap between scans, a global registration was implemented, which allowed all scans except for the mobile scan data to be adjusted simultaneously for a better fit. However, to improve reliability, the leveling values from the scanner remained fixed during all stages of the adjustment. RMS residuals between scans typically ranged from 10-20 cm. Cloud to cloud methods require much less field time compared to target methods, although they can sometimes result in reduced accuracy (Williams *et al.* 2012), particularly over long distances when a geo-referenced, baseline surface is not available. Fortunately, the mobile scan data provided the necessary baseline. Several quality control measures were performed to evaluate the data alignment quality including cross sections, examining point blending, and calculating RMS values between adjacent scans (Olsen, 2011).

The static scan origins determined from the cloud-to-cloud adjustment were then compared to the uncorrected GPS data obtained for the scans to determine the translation and rotation parameters necessary for a similarity transformation of the data into the Japanese Geodetic Datum 2000 Zone 10 coordinate system using least squares. This produced a RMS of 2.2 m between the uncorrected GPS data and the static scan origins determined from the cloud-to-cloud adjustment.

c. Topographic filtering

The data was topographically filtered to remove buildings and other noise. The topographic filter performs statistical analysis of all points in a grid cell size and selects the lowest point to represent the topography. A cell size of 5 m was used for this dataset. However, much finer resolution could be obtained for a significant amount of the dataset. Following the filter, the data was verified to ensure building points did not remain in areas where there might have not been any topographic points. Figure 6(b) shows the topographic-filtered point cloud for part of the central section. Figure 7 shows the final point cloud modeling the topography throughout most of the valleys of Onagawa.

d. Coordinate transformation

The mobile scan data and uncorrected GPS data contained ellipsoid heights, which do not reflect elevation above mean sea level. The processed data was converted to orthometric heights using the GSIGEO2000 Geoid model, enabling the data to be suitable for tsunami inundation modeling. Finally, the data was re-projected into WGS84 geographic coordinates using GIS.

e. Creation of a DEM

The XYZ point data was then binned and converted to a Digital Elevation Model (DEM) in a grid format using tools available through the Generic Mapping Tools (Wessel and Smith, 1991). This process includes filling small holes in the data through interpolation techniques for a seamless model. This DEM can then be fed into the tsunami modeling for another level of detail for a specific site.

DETERMINISTIC TSUNAMI LOAD PREDICTION

Japan has been the leading country in tsunami research because of the frequent and imminent threat it has experienced since the twentieth century. Only following the 2004 Indian Ocean Tsunami have other countries, including the US, significantly increased their research efforts, particularly with laboratory research. However, due to the complexity of the physical phenomenon of tsunami and the lack of high-performance computational capabilities, there is still a noticeable lack of research efforts in numerical modeling and simulation of the effects of tsunami impact on a structure, especially regarding fluid-structure interaction. Recently, researchers at the Port and Airport Research Institute (PARI), Japan have been developing in-house, tsunami-structure interaction models using CADMUS-SURF and STOC. Other researchers, including those at Oregon State University and the University of Hawaii in the US, and at Nagoya University in Japan, have used the multi-physics code LS-DYNA for this purpose. Most of the numerical studies so far have focused on modeling laboratory-scale, rather than regional scale cases.

Since 2005, Yim's research group at Oregon State University, in collaboration with researchers at the University of Hawaii at Manoa, has conducted two numerical studies for the Oregon Department of Transportation on tsunami loads on full-scale coastal bridges including the Spencer Creek Bridge directly north of Newport, OR (Nimmala *et al.* 2006) and four other bridges around the Siletz Bay (Yim *et al.* 2011). The input tsunami flow fields to the numerical fluid-structure interaction model were developed based on numerical simulation of 500-year Cascadia events (Cheung *et al.*, 2011). Even with high-performance computation facilities, these studies are limited to two-dimensional cross sections due to the large physical scale (tens to hundreds of meters in each dimension) and long loading time history (hundreds to thousands of seconds). To date, the full-scale numerical simulation results have not been calibrated due to a lack of suitable field data. However, with the availability of

the quantitative information obtained from the post-event assessment of tsunami impact and the LIDAR survey of tsunami-induced structural damage measurement, calibration of these full-scale fluid-structure contact/impact numerical models may now be possible.

Definition of the overland flow conditions from the 2011 Tohoku tsunami is the first step in the calibration process. Modeling of tsunami inundation requires high-resolution topography and bathymetry near the coast. In addition to the LIDAR topography we gathered at Onagawa, aerial LIDAR data for Sendai is publicly available from the Geospatial information Authority of Japan. These high-resolution LIDAR datasets are merged with the 50-m resolution DEM from the same agency. The digital coastline and depth contour data from Japan Hydrographic Association defines the nearshore bathymetry, which in turn is blended into the JMA regional and ETOPO1 global datasets already in geodetic coordinates using the WGS84 datum. Inundation mapping may be performed under bare-earth conditions with grid size up to 30 m. If buildings are included, the DEM should have a resolution of at least 3 m to capture flow acceleration in built environment, which is achievable through LIDAR data. The runup data of Mori et al. (2011) will allow validation of the modeled tsunami.

With the near-field tsunami correctly reproduced and near-shore topography obtained from the LIDAR survey, a post-event analysis will allow validation of the procedure for deterministic load prediction as follows:

a. Select a structure in Onagawa or Sendai where LIDAR data of the damage is available.
b. Develop a numerical model of the structure using as-built data from construction documents and verify the modeling prediction with the LIDAR data.
c. Obtain a flow time history of the surface elevation and velocity from numerical modeling of the Tohoku tsunami.
d. Perform a simulation of tsunami flow impact on the selected structure using a numerical procedure such as the one presented in Yim *et al.* (2011) for both the runup and drawdown of the largest wave at the site. The effects of coupled fluid-structure interaction should also be included in the model.
e. Validate the numerical prediction of terminal structural response by comparing it to measured values from the LIDAR data.

The LIDAR field data, however, provides information on the final (damaged) condition of the structures; it cannot be used to validate the time histories of the simulated structural responses. This raises the level of uncertainties in estimating the physical properties of the structure and limits the confidence level of model numerical validation. To fill this time history data gap and improve our deterministic tsunami load estimation calibration process, laboratory-scale model experiments of the selected structures and tsunami loading conditions should be conducted to provide data for structural properties estimation, time history responses and validation of the final (damaged) structural configurations. These laboratory experiments should be designed based on the field inundation and structural damage information, as well and preliminary simulation results of both tsunami inundation and coupled fluid-structure-interaction models. It should be pointed out that because of scaling effects, the laboratory experiments are to be designed to elucidate certain nonlinear behavior of structural members or sections only, and not the entire structure under consideration. A scaled building would not respond dynamically in the laboratory because of its very small time scale comparing to the tsunami. It would basically be a quasi-static process in the building response.

PROBABILIISTIC TSUNAMI HAZARD ASSESSMENT

Probabilistic models are becoming popular for tsunami hazard assessment, but few of these models

have been fully calibrated with an actual event. The Tohoku tsunami is estimated to have a return period of 1,000 years based on sediment records and slip rates (Minoura *et al.*, 2001). The successful reproduction of the near-field tsunami combined with the high-resolution LIDAR data of the topography and observed infrastructure damage provide a unique opportunity to calibrate a probabilistic model for improved tsunami hazard assessment.

The first step in a tsunami hazard assessment is to define the tsunamigenic sources. Japan has experienced several tsunamis from around the Pacific Rim, but the most destructive events have been generated locally along the Japan-Kuril-Kamchatka-Kuril subduction zone. Yamazaki *et al.* (2006) delineated and discretized the subduction zones into a system of rectangular subfaults and compiled the corresponding tectonic parameters. The data were originally developed to generate a database of tsunami Green functions for a forecast algorithm, but they can also be used to define the source mechanisms of tsunami events. A logic tree approach can provide a sample of tsunamigenic earthquakes and their occurrence probabilities from tectonic, geodetic, historical, and paleo-tsunami data. The logic tree also systematically subdivides the occurrence probability to account for variations in the magnitude, fault geometry, and location of each event.

The change in landforms from coseismic deformation is negligible compared to the spatial scale of a destructive tsunami. The DEM based on the current and best-available data is valid for probabilistic modeling of tsunami events. The tide level provides another source of uncertainties, which can be represented by a statistical distribution determined from the constituents near the site. However, the need to consider multiple water levels substantially increases the number of events to be considered in the probabilistic analysis. For a conservative approach, the mean-higher-high-water (MHHW) level or the mean-sea (MS) level with an appropriate increment can be used instead of considering multiple water levels.

We may then reconstruct statistical distribution of tsunami amplitude at near-shore waters for general hazard assessment (e.g., Thio *et al.*, 2010; Uslu *et al.*, 2010). Since a Green function approach based on a linear model is typically used to compute near-shore wave amplitude, it is important that the projected wave amplitude for a given return period is an order of magnitude less than the water depth. The analysis can also be performed at a region of interest to produce probabilistic hazard maps. Site-specific hazard analysis requires a reconstruction of statistical distributions of flow parameters such as depth, velocity, and flux at the site for hazard mapping or engineering design (*e.g.*, Craw, 2008; González *et al.*, 2009; Priest *et al.*, 2009; Ge and Cheung, 2011). One would analyze each tsunami event to determine representative parameters such as maximum amplitude, depth, velocity, and flux. Probabilistic flow parameters can be developed in near-shore waters or at the site itself from the sample of computed tsunamis and their occurrence probabilities. Note that these flow parameters, such as depth and velocity, are not coincidental for a given return period, and should not be combined to determine structural loads.

Unfortunately, the time history of a tsunami event, which might be crucial for load definition, is lost in the development of probabilistic design parameters. Alternately, the sample of computed tsunami events can be used directly to determine probabilistic design loads on a structure (*e.g.*, Cheung *et al.*, 2011). This process involves extraction of the flow depth and velocity time series at the site from each computed tsunami and application of the flow depth and velocity time series in a physics-based model to determine the maximum anticipated load on the structure for each tsunami event. This method also enables reconstruction of the statistical distributions of the design loads from the computed values and the occurrence probabilities associated with the tsunami events. Comparison of the recorded inundation and structural damage at Onagawa and Sendai with the projected 1,000-year event will validate the probabilistic tsunami hazard model for application at other locations along the coastlines of Japan.

CONCLUDING REMARKS

This paper outlines the necessary steps to use advanced numerical modeling and geospatial data to

obtain probabilistic design loads for tsunamis. An analysis plan to develop an improved understanding of tsunami loads on structures through estimations using these observations and analyses is described. Advanced modeling efforts of the tsunami following an event were first summarized. Next, the acquisition and processing of ground-based LIDAR data for topographic mapping and analyses was discussed. The LIDAR data provides the critical geospatial information to link field observations, topographic mapping, and structural damage to feed and validate numerical models. The dense quantity of measurements enables one not only to virtually explore the site, but also improves quantification of damage. In addition to the tsunami modeling and LIDAR data collection and analysis, the plan also includes immediate, specific deterministic analysis and laboratory-scale experiments needed to calibrate inundation models for built environment and a probability-based tsunami design methodology integrating the above information. A designer can then implement this methodology to incorporate potential tsunami impacts.

ACKNOWLEDGMENTS

Funding for the survey was provided by the National Science Foundation through NSF Rapid Grants Nos. 1138710 and 1138699. We thank Dr. T. Kuwayama for supplying the 20 arc-sec Japan bathymetry data, the Port and Airport Research Institute (PARI), Japan for providing the near-shore wave buoy data, Leica Geosystems and Maptek I-Site for providing data-processing software, and Asia Air Survey, Co., Japan for supplying the mobile laser scan data used in this project. Evon Silvia and Shawn Butcher (Oregon State University), Lyle Carden (Martin & Chock, Inc.), Shinya Tachibana (Saitama University), and several Building Research Institute (BRI) collaborators led by Yasuo Okuda assisted with the field work. Ian Robertson (University of Hawaii, Manoa) and Gary Chock (Martin & Chock, Inc.) provided guidance to the field effort.

REFERENCES

Cheung, K.F., Wei, Y., Yamazaki, Y., and Yim, S.C.S. (2010). "Modeling of 500-year tsunamis for probabilistic design of coastal infrastructure in the Pacific Northwest," Coastal Eng., 58(10), 970-985.

Craw, M.L. (2008). "Probabilistic Approach for Tsunami Inundation Mapping," MS Thesis, University of Hawaii, Honolulu.

Ge, L. and Cheung, K.F. (2011). "Spectral sampling method for uncertainty propagation in long-wave runup modeling," J. Hyd. Eng., 137(3), 277-288.

González, F.I., *et al.* (2009). "Probabilistic tsunami hazard assessment at Seaside, Oregon, for near- and far-field seismic sources," J. Geophys. Res., 114, C11023, doi: 10.1029/2008JC 005132.

Ito, Y., T. Tsuji, Y. Osada, M. Kido, D. Inazu, Y. Hayashi, H. Tsushima, R. Hino, and H. Fujimoto (2011). "Frontal wedge deformation near the source region of the 2011 Tohoku-Oki earthquake," Geophys. Res. Lett., 38, L00G05, doi:10.1029/2011 GL048355.

Kayen, R., Stewart, J.P., Collins, B., (2010). "Recent advances in terrestrial LIDAR applications in geotechnical earthquake engineering," 5th Int. Conf. on Recent Advances in Geotechnical Earthquake Engrg and Soil Dynamics, San Diego, CA, 2010.

Kayen, R., Tanaka, Y., Tanaka, H., Sugano, T., Estevez, I.A., Cullenward, S.S., Yeh, W., and Thomas, D., (2011), "LIDAR and Field Investigation of the March 11, 2011 M9.0 Great Tohoku Offshore Earthquake, and April 7, 2011 M7.4 Aftershock," Geotechnical Reconnaissance of the 2011 Tohoku Japan earthquake, Quick Report 6, GEER Association Report #GEER-025f.

Messinger, D.W., van Aardt, J., McKeown, D., Casterline, M., Faulring, J., Raqueño, J., Basener, B., and Velez-Reyes, M., (2010), "High-resolution and LIDAR imaging support to the Haiti earthquake relief effort," Proc. SPIE 7812, 78120L; doi:10.1117/12.862090

Minoura, K.; Imamura F., Sugawara D., Kono Y. & Iwashita T. (2001). “The 869 Jōgan tsunami deposit and recurrence interval of large-scale tsunami on the Pacific coast of northeast Japan,” J. Natural Disaster Science, 23(2): 83–88.

Nimmala, S., Yim, S.C., Cheung, K.F. and Wei, Y., “Tsunami Design Criteria for Coastal Infrastructure: A Case Study for Spencer Creek Bridge, Oregon,” Technical Report, Salem: Oregon Department of Transportation, 2006.

Mori, N., T. Takahashi, T. Yasuda, and H. Yanagisawa (2011), “Survey of 2011 Tohoku earthquake tsunami inundation and run-up,” Geophys. Res. Lett., 38, L00G14, doi: 10.1029/2011GL049210.

Okada, Y. (1985). “Surface deformation due to shear and tensile faults in a half space,” Bull. Seismol. Soc. Am., 75(4), 1135-1154.

Olsen, M.J., Kuester, F., Chang, B., and Hutchinson, T., 2010. “Terrestrial laser scanning based structural damage assessment,” J. Comp. Civil Eng., 24(3), p. 264-272.

Olsen, M.J., (2011). “Putting the pieces together: laser scan geo-referencing,” LIDAR Magazine, 1(2).

Olsen, M.J., Donahue, J., (2011). “A wave of new information: LIDAR investigations of the 2009 Samoan tsunami,” in ASCE Solutions to Coastal Disasters Conference, Anchorage, Alaska.

Olsen, M.J., Piaskowy, S., Yim, S., Burgos, L., and Butcher, S.M., (2011). “LIDAR investigations of the 2010 Maule Chile Earthquake,” in the 6th Int. Structural Engineering and Construction (ISEC-6), Modern Methods and Advances in Structural Engineering and Construction, Zurich Switzerland.

Olsen, M.J., Cheung, K.F., Yamazaki, Y., Butcher, S., Garlock, M., Yim, S., Piaskowy, S., Robertson, I., Burgos, L., and Young, Y.L., (2012a). “Damage assessment of the 2010 Chile earthquake and tsunami using terrestrial laser scanning,” Earthquake Spectra, accepted pending revisions.

Olsen, M.J., Carden, L., Silvia, E.P., Chock, G., Robertson, I.N., & Yim, S. (2012b). “Capturing the impacts: 3D laser scanning following the Tohoku earthquake and tsunami,” Proceedings of the 9th CUEE and 4th ACEE Joint Conference, Tokyo Institute of Technology, Japan.

Priest, G.R., Goldfinger, C., Wang, K., Witter, R.C., Zhang, Y., and Baptista, A.M. (2009). “Confidence levels for tsunami-inundation limits in northern Oregon inferred from a 10,000-year history of great earthquakes at the Cascadia subduction zone,” Natural Hazards, 54(1), 27-73.

Simons, M., S.E. Minson, A. Sladen, F. Ortega, J. Jiang, S.E. Owen, L. Meng, J.-P. Ampuero, S. Wei, R. Chu, D.V. Helmberger, H. Kanamori, E. Hetland, A.W. Moore, and F.H. Webb (2011). “The 2011 magnitude 9.0 Tohoku-oki earthquake: Mosaicking the megathrust from seconds to centuries,” Science, 332(6036), 1421-1425.

Thio, H.K., Somerville, P., and Polet, J. (2010). Probabilistic Tsunami Hazard in California. Pacific Earthquake Engineering Research Center, PEER Report 2010/108, University of California, Berkeley.

Uslu, B., Titov, V.V., Eble, M., and Chamberlin, C.D. (2010). Tsunami Hazard Assessment for Guam. NOAA Pacific Marine Environmental Laboratory Special Report, Seattle, Washington.

Vosselman, G., and Maas, H.G., (2010), “Airborne and Terrestrial Laser Scanning,” Whittles Publishing, Scotland, UK, 320 p.

Wessel, P., and Smith, W.H.F. (1991), "Free software helps map and display data," EOS Trans. AGU, 72, 441, 445-446.

Williams, K.E., Olsen, M.J., and Chin, A., (2012), “Accuracy assessment of geo-referencing methodologies for terrestrial laser scan surveys,” Proceedings of the ASPRS annual conference.

Yamazaki, Y. and Cheung, K.F. (2011). “Shelf resonance and impact of near-field tsunami generated by the 2010 Chile earthquake,” Geophys. Res. Lett., 38, L12605, doi: 10.1029/2011GL047508.

Yamazaki, Y., Cheung, K.F., and Kowalik, Z. (2011a). “Depth-integrated, non-hydrostatic model with grid nesting for tsunami generation, propagation, and run-up,” Int. J. Num. Meth. Fluids, 67(12), 2081-2107..

Yamazaki, Y. and K.F. Cheung (2011) “Shelf resonance and impact of near-field tsunami generated by the 2010 Chile earthquake,” Geophys. Res. Lett., 38, L12605, Doi: 10.1029/2011GL047508.

Yamazaki, Y., Z. Kowalik, and K.F. Cheung (2009). “Depth-integrated, non-hydrostatic model for wave breaking and runup,” Int. J. Num. Meth. Fluids, 61(5), 473-497.

Yamazaki Y., Lay, T., Cheung, K.F., Yue, H., and Kanamori, H. (2011b). Modeling near-field tsunami observations to improve finite-fault slip models for the 11 March 2011 Tohoku earthquake. Geophys. Res. Lett., 38, L00G15, Doi: 10.1029/2011GL049130

Yamazaki, Y., Wei, Y., Cheung, K.F., and Curtis, G.D. (2006). "Forecast of tsunamis from the Japan-Kuril-Kamchatka source region," Natural Hazards, 38(3), 411-435.

Yim, S.C., Boon-Intra, S. Nimmala, S.B., Winston, H.M. and Cheung, K.F. (2011). "Development of a Guideline for Estimating Tsunami Forces on Bridge Superstructures," Technical Report, Oregon Department of Transportation.

Zhao, D., Z. Huang, N. Umino, A. Hasegawa, and H. Kanamori (2011). "Structural heterogeneity in the megathrust zone and mechanism of the 2011 Tohoku-oki earthquake (Mw 9.0)," Geophys. Res. Lett., 38, L17308, doi:10.1029/2011GL048408.

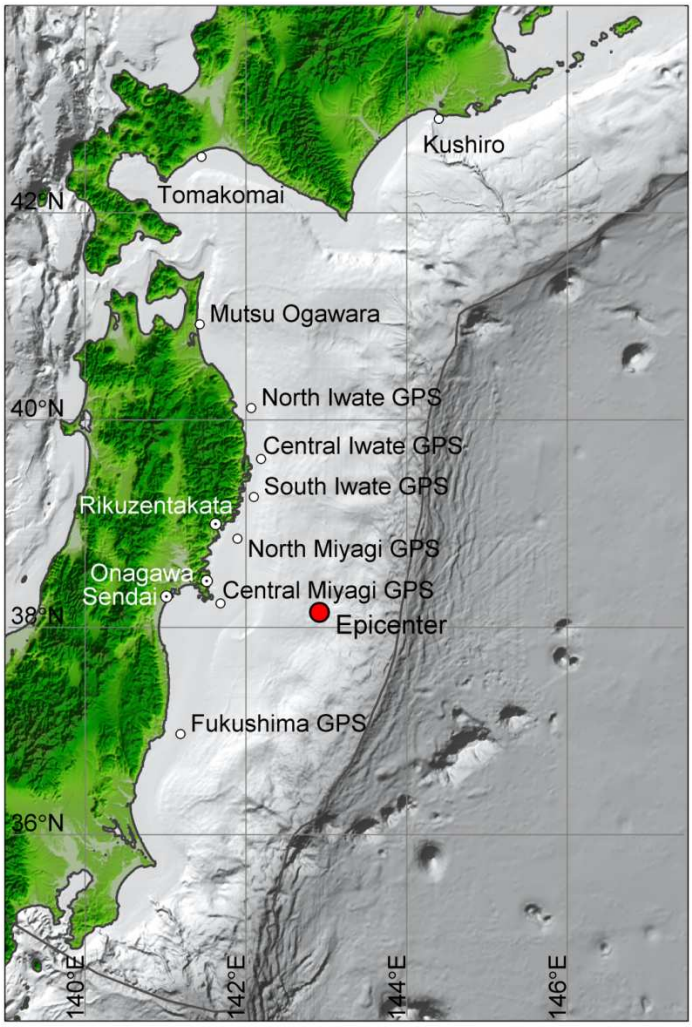

Fig. 1 Map depicting the general topography and bathymetry, the epicenter of the Tohoku earthquake, and locations of near-shore buoys.

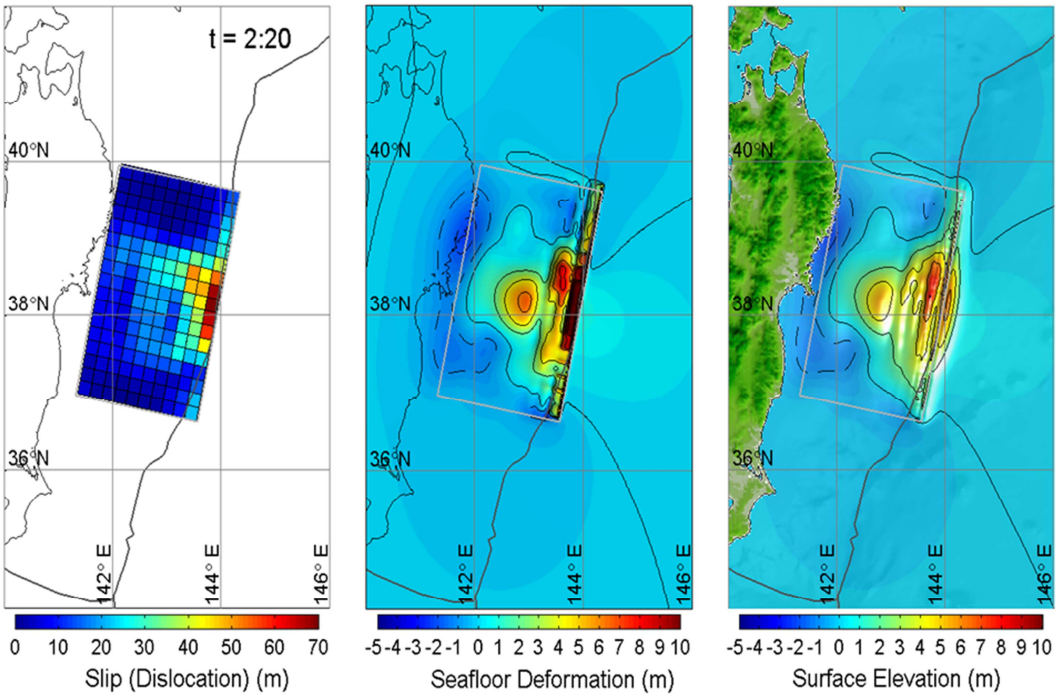

Fig. 2 Slip distribution, seafloor deformation, and tsunami waves at the end of the rupture.

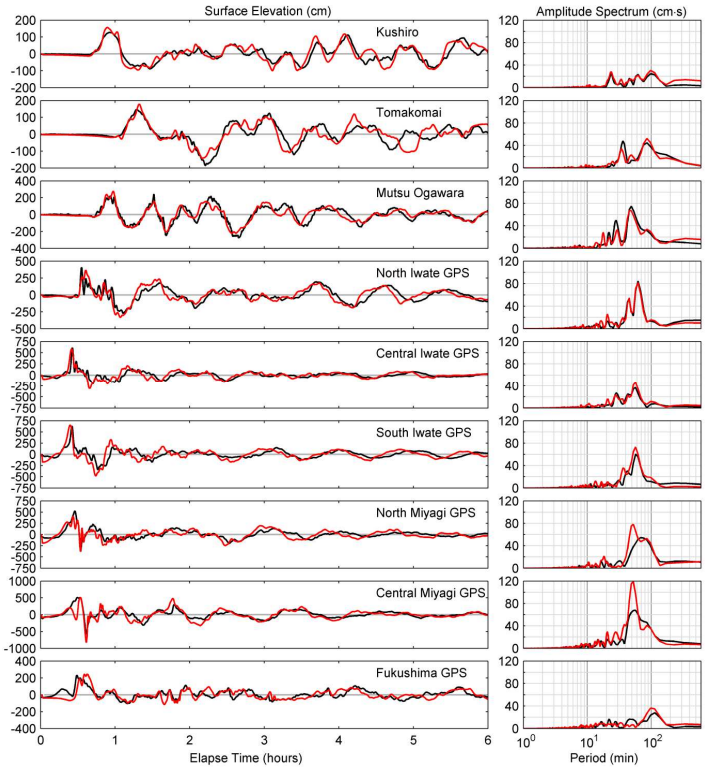

Fig. 3 Computed (red) and measured (black) tsunami signals at near-shore buoys along the Tohoku and Hokkaido coasts.

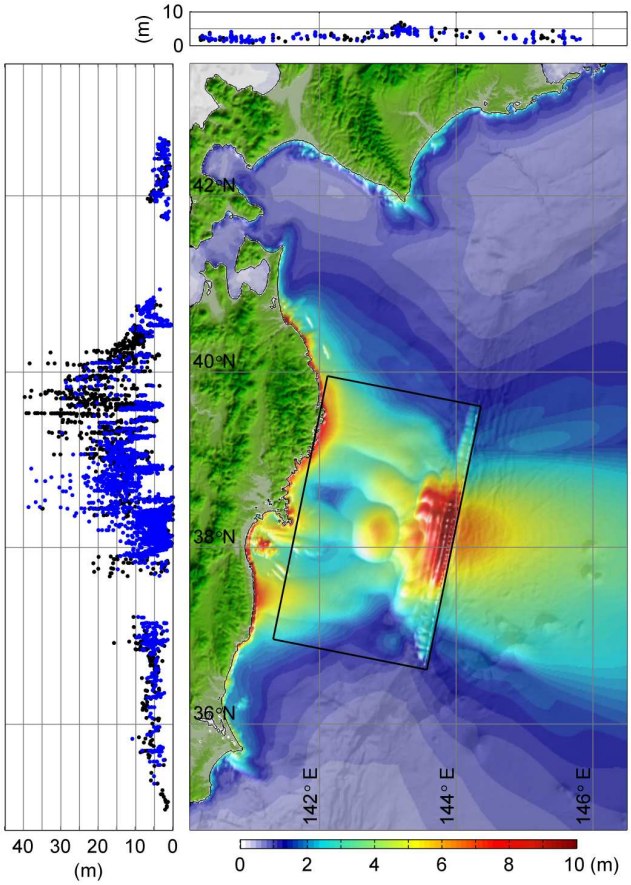

Fig. 4 Computed surface elevation and recorded runup of the Tohoku tsunami. Black and blue dots indicate measured runup and surface elevation from MSL.

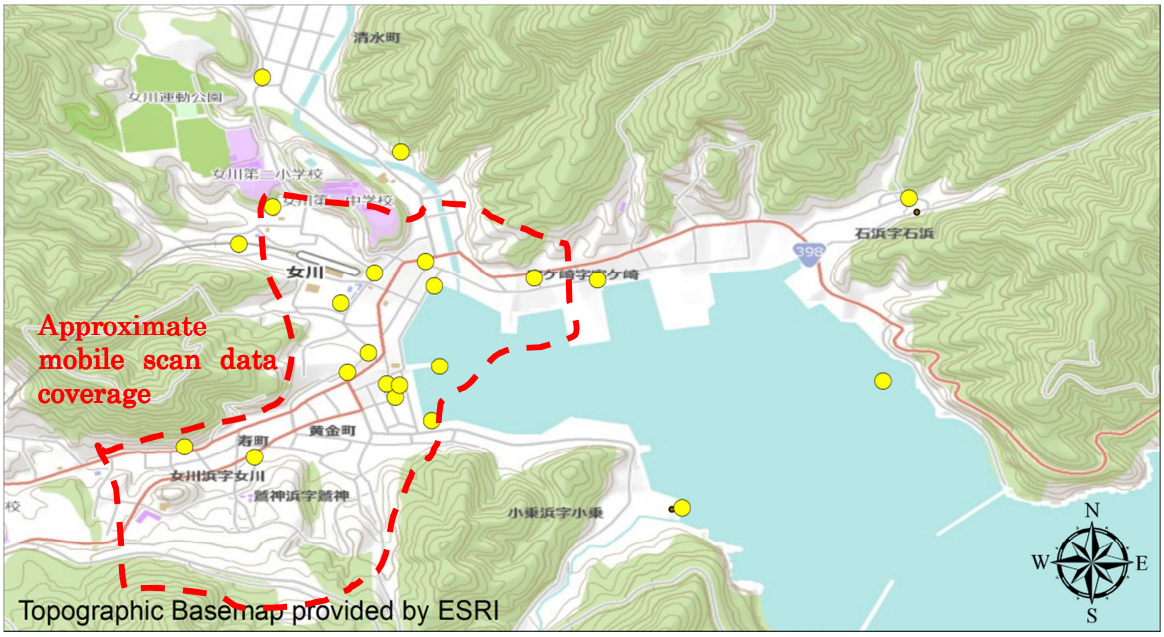

Fig. 5 Scan locations (yellow circles) in Onagawa for topographic mapping. The red-dashed line represents the approximate extents of mobile laser scan data provided by Asia Air Survey, Co.

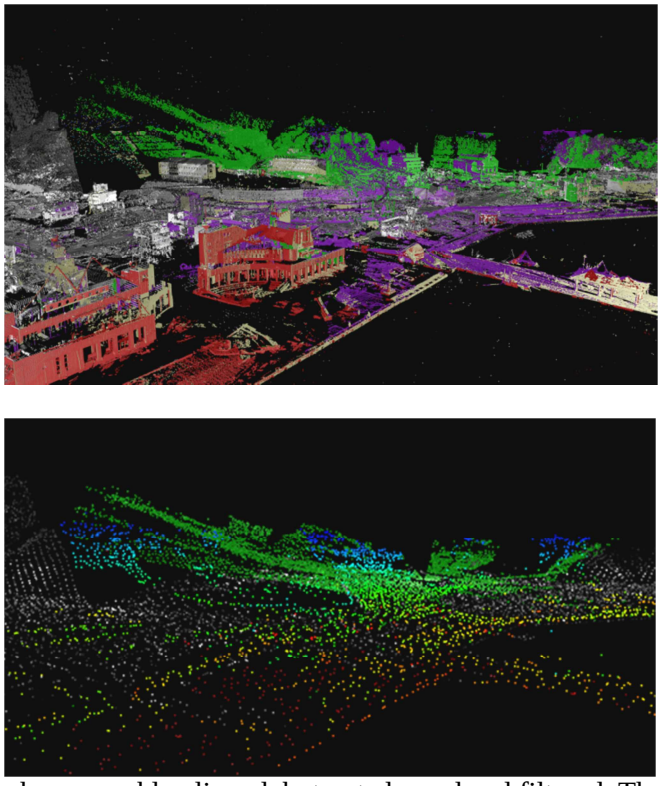

Fig. 6 Scans that have been roughly aligned, but not cleaned and filtered. The grayscale data are mobile laser scan data provided by Asia Air Survey, Co. (a) The colored scans are some of the static scans, each colored a different color; and (b) Data points following topographic filtering.

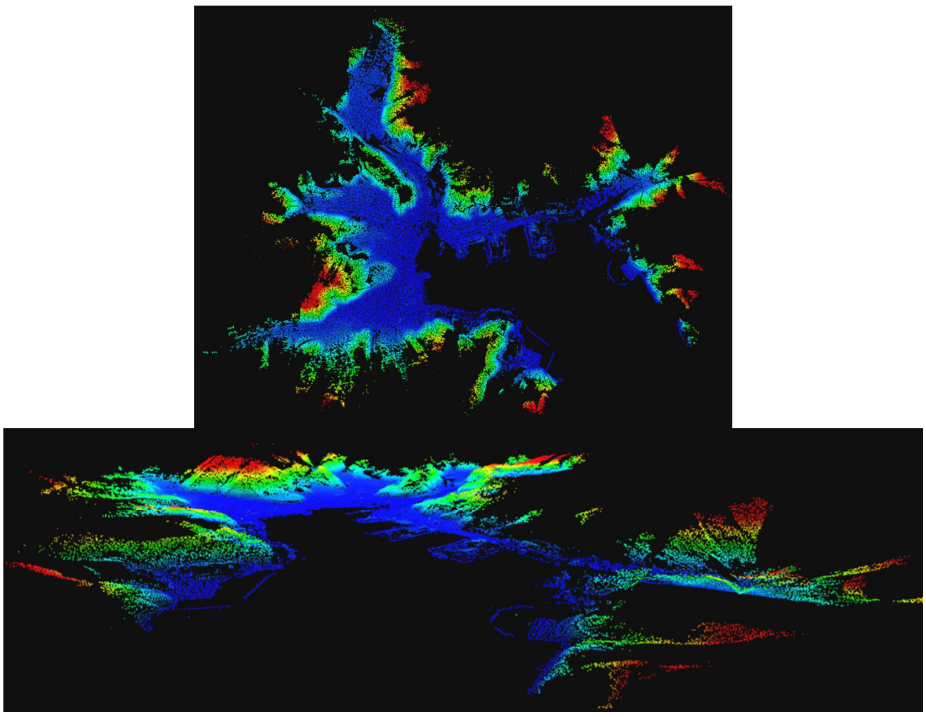

Fig. 7 (a) Plan view and (b) Oblique view of processed LIDAR topographic data, colored by elevation. (Blue = low elevation (0 m) and Red = high elevation (>100 m))